Supporting Information

Fine tuning of Fermi level by charged impurity-defect cluster formation and thermoelectric properties in n-type PbTe based compounds

Min Ho Lee,[a,b] Sungjin Park,[c] Jae Ki Lee,[c] Jaywan Chung,[c] Byungki Ryu,[c,†] Su-Dong Park,[c] and Jong-Soo Rhyee[a,*]

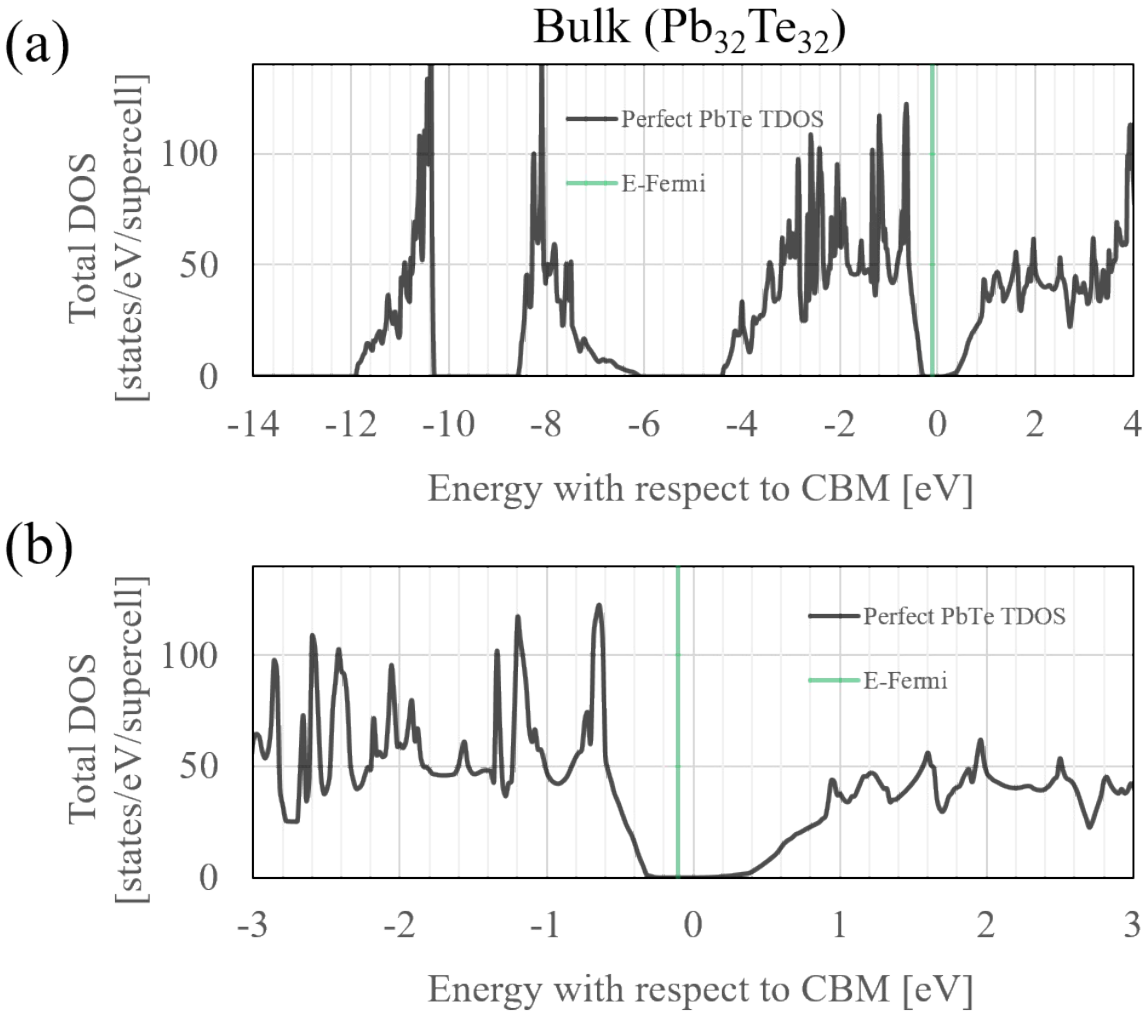

Fig. S1. Total density of states of pristine PbTe ($Pb_{32}Te_{32}$) with full scale (a) and near the Fermi level (b), where sky blue line is the Fermi level.

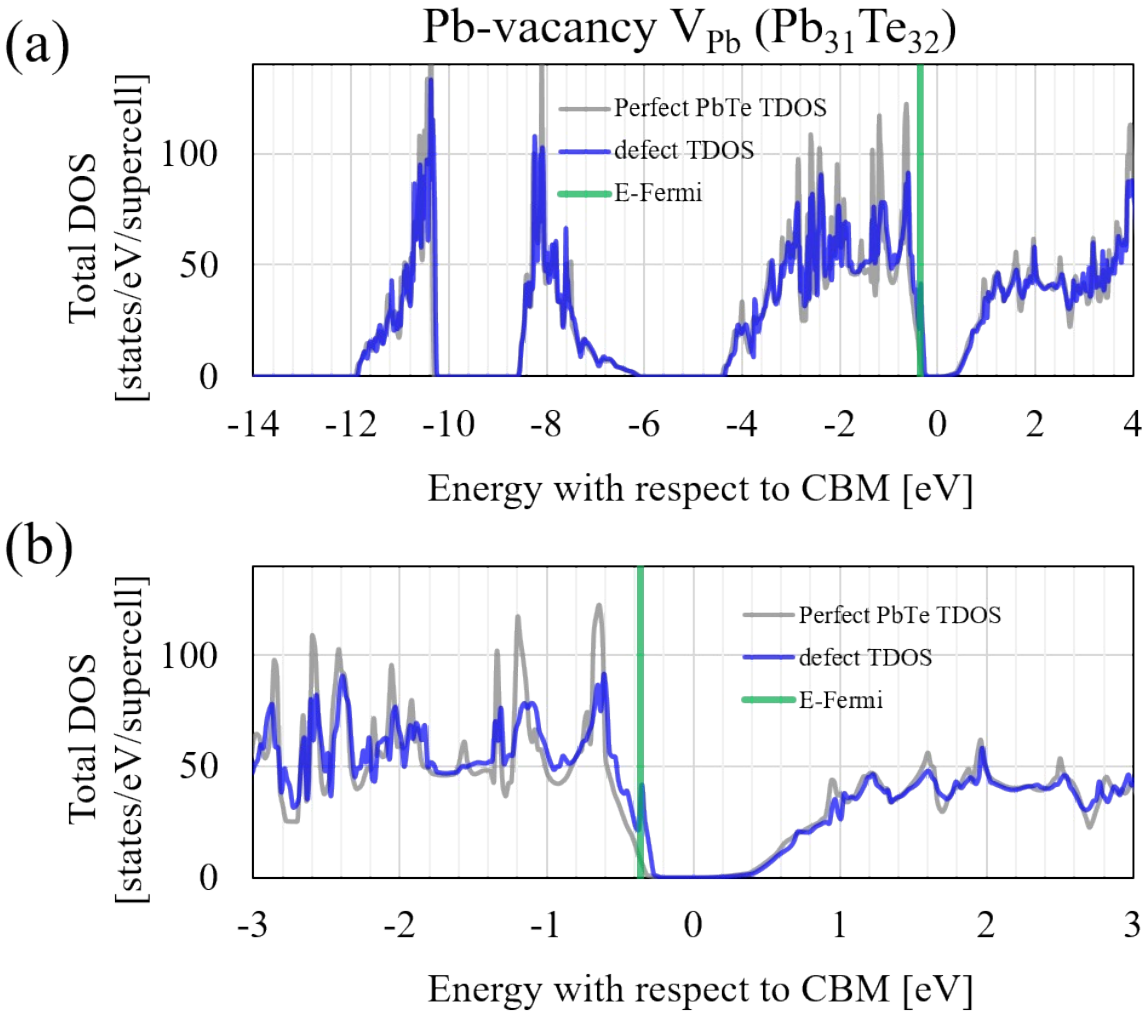

Fig. S2. Total density of states of Pb vacant PbTe ($Pb_{31}Te_{32}$, blue line) with pristine PbTe (gray line) for comparison with full scale (a) and near the Fermi level (b), where sky blue line is the Fermi level.

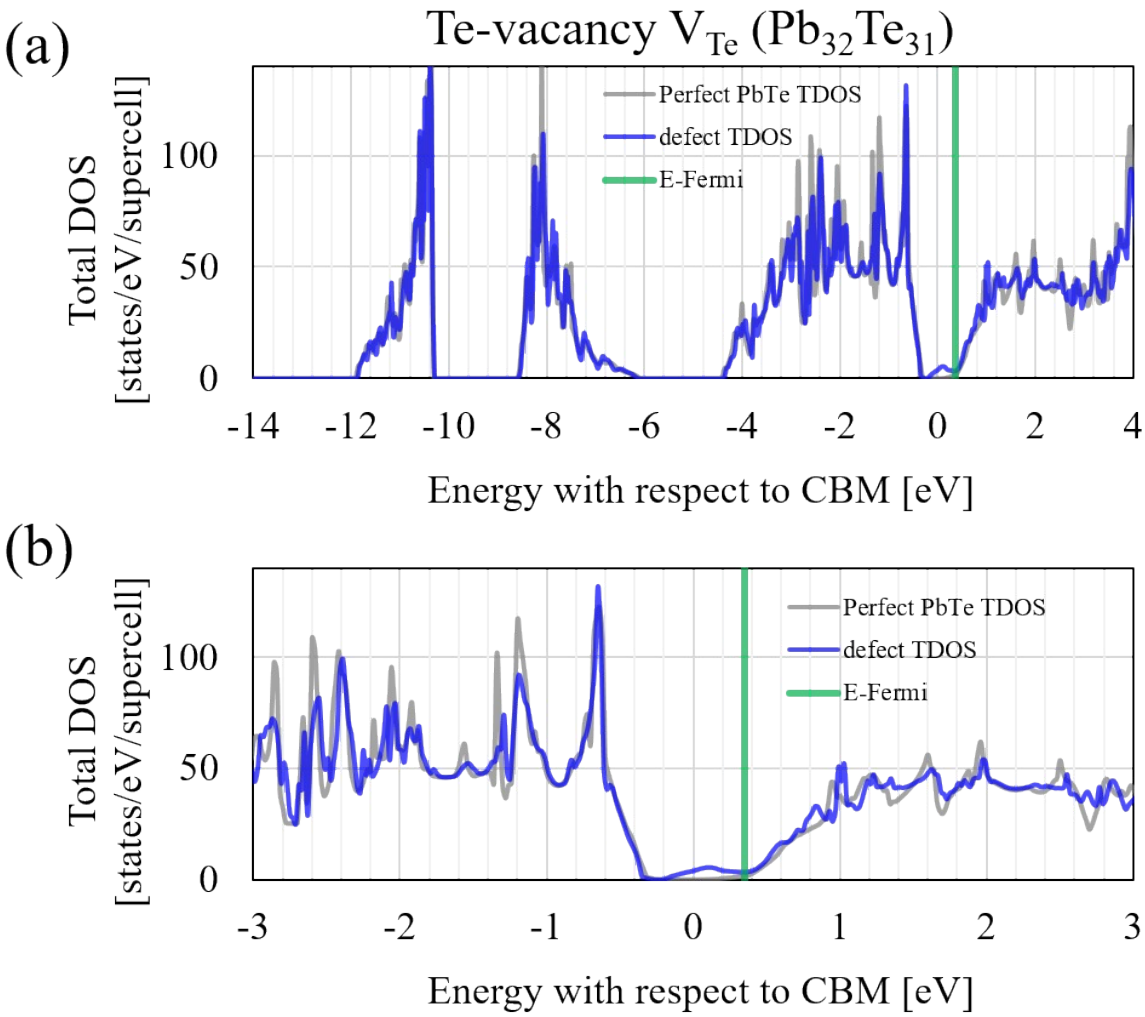

Fig. S3. Total density of states of Te vacant PbTe ($Pb_{32}Te_{31}$, blue line) with pristine PbTe (gray line) for comparison with full scale (a) and near the Fermi level (b), where sky blue line is the Fermi level.

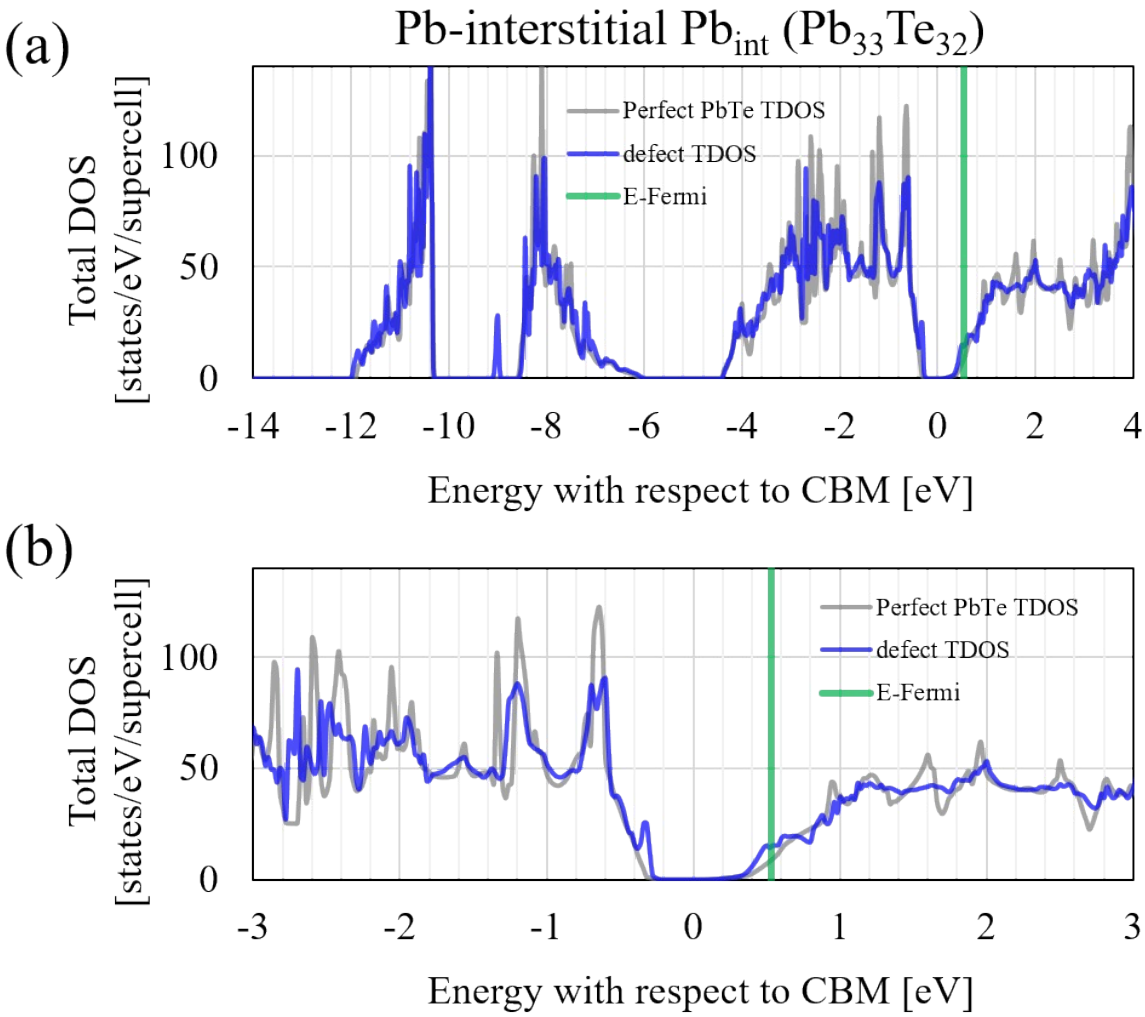

Fig. S4. Total density of states of Pb interstitial doping in PbTe ($Pb_{33}Te_{32}$, blue line) with pristine PbTe (gray line) for comparison with full scale (a) and near the Fermi level (b), where sky blue line is the Fermi level.

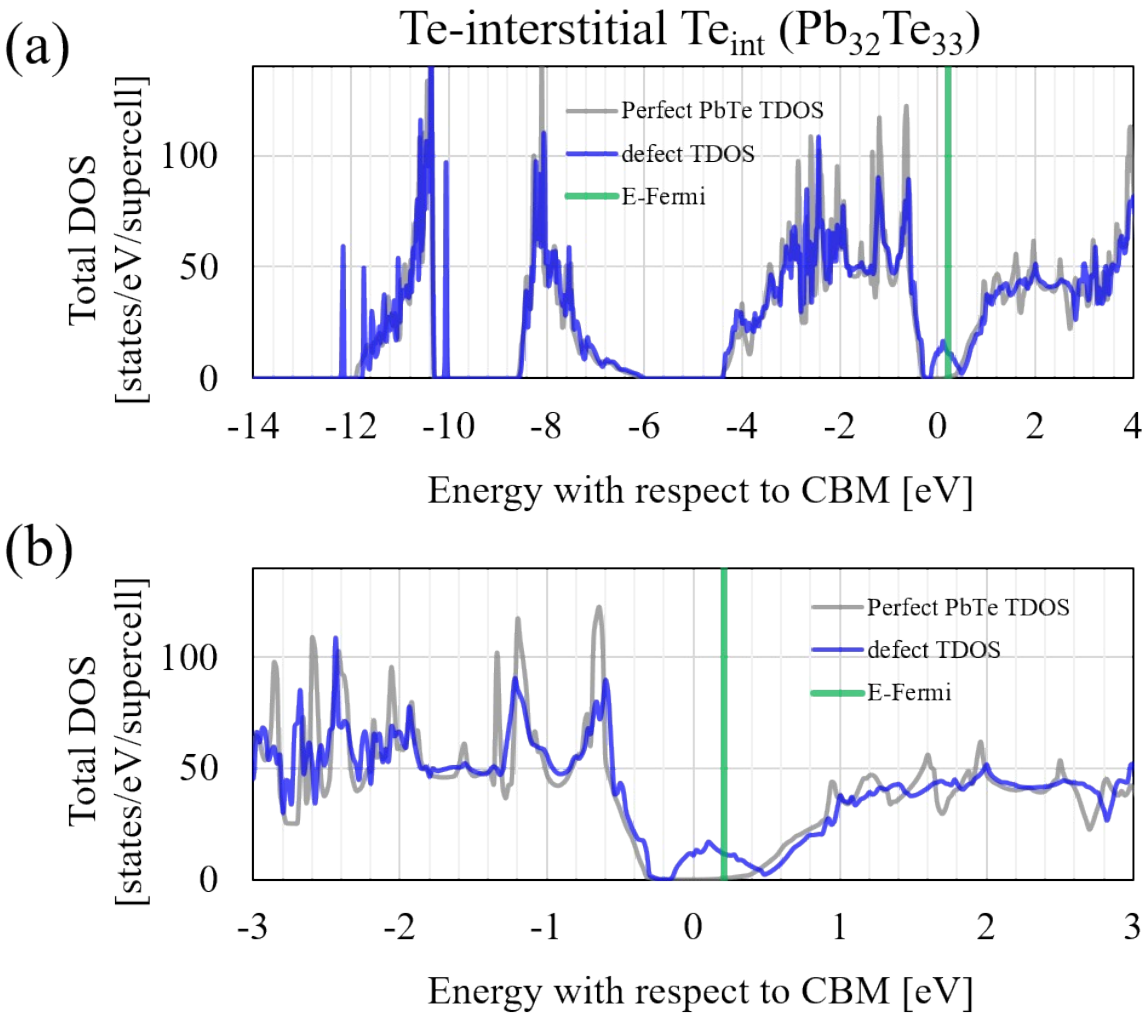

Fig. S5. Total density of states of Te interstitial doping in PbTe ($Pb_{32}Te_{33}$, blue line) with pristine PbTe (gray line) for comparison with full scale (a) and near the Fermi level (b), where sky blue line is the Fermi level.

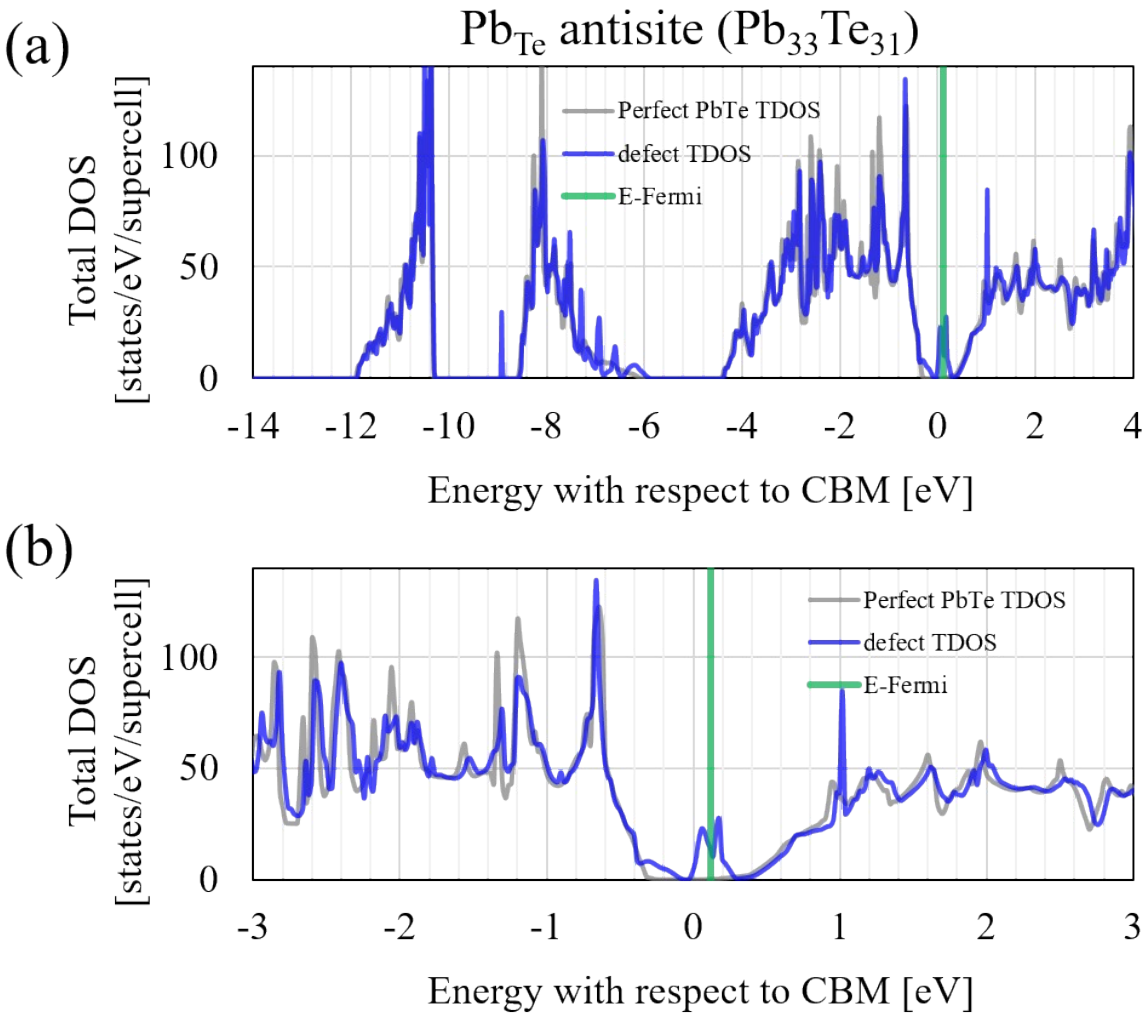

Fig. S6. Total density of states of Pb antisite defect at Te-site in PbTe ($Pb_{33}Te_{31}$, blue line) with pristine PbTe (gray line) for comparison with full scale (a) and near the Fermi level (b), where sky blue line is the Fermi level.

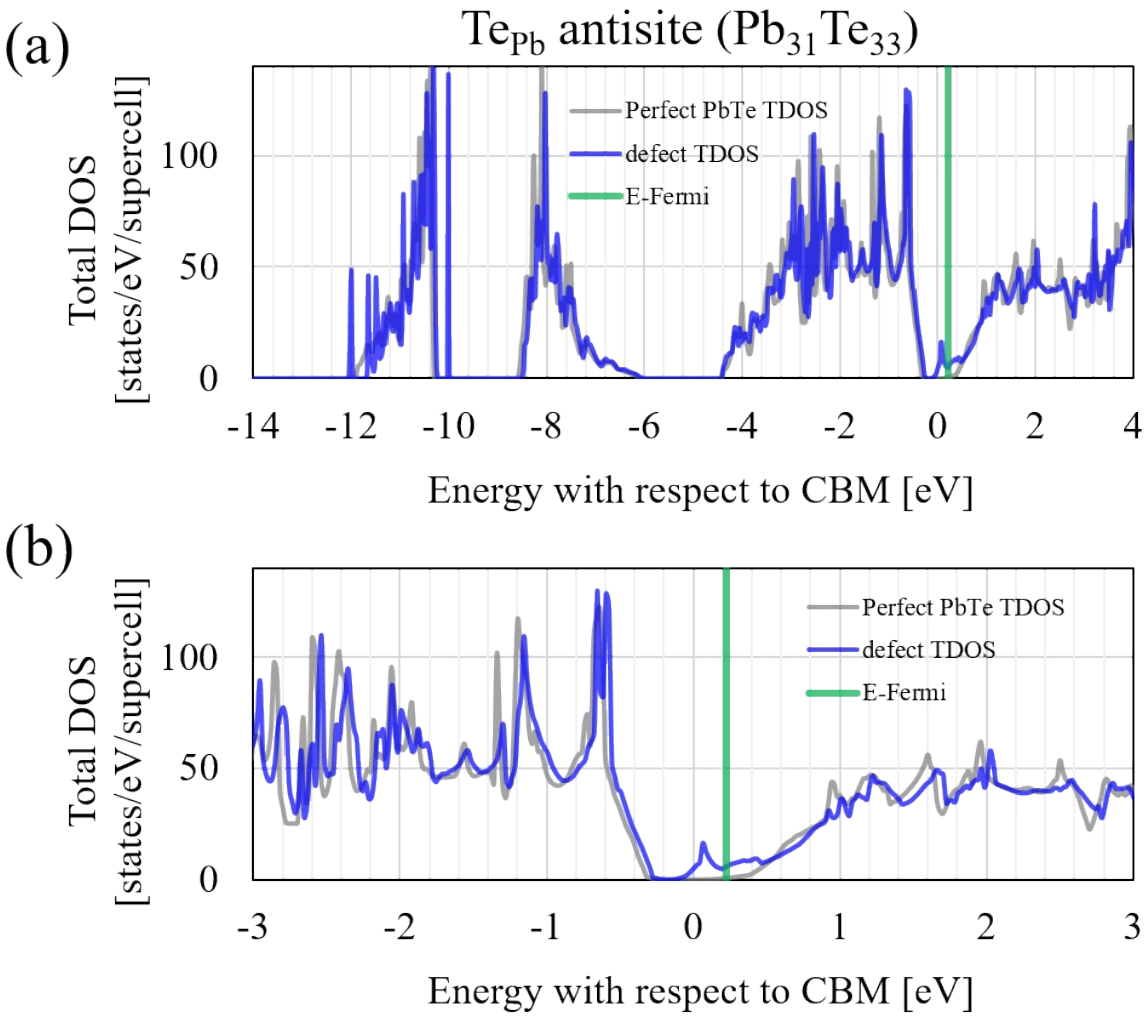

Fig. S7. Total density of states of Te antisite defect at Pb-site in PbTe ($Pb_{31}Te_{33}$, blue line) with pristine PbTe (gray line) for comparison with full scale (a) and near the Fermi level (b), where sky blue line is the Fermi level.

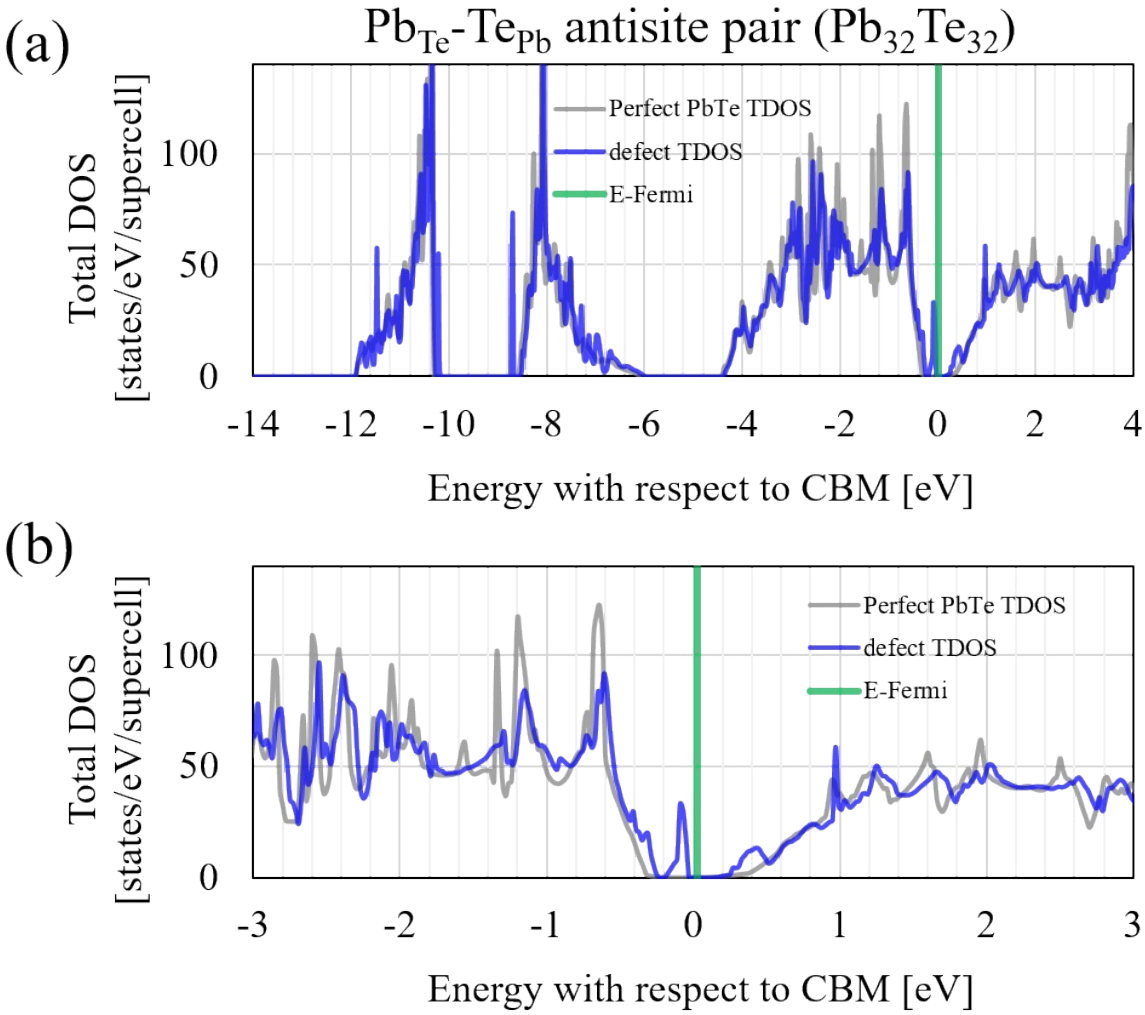

Fig. S8. Total density of states for antisite defect pairs of Pb_{Te} and Te_{Pb} in PbTe ($Pb_{32}Te_{32}$, blue line) with pristine PbTe (gray line) for comparison with full scale (a) and near the Fermi level (b), where sky blue line is the Fermi level.

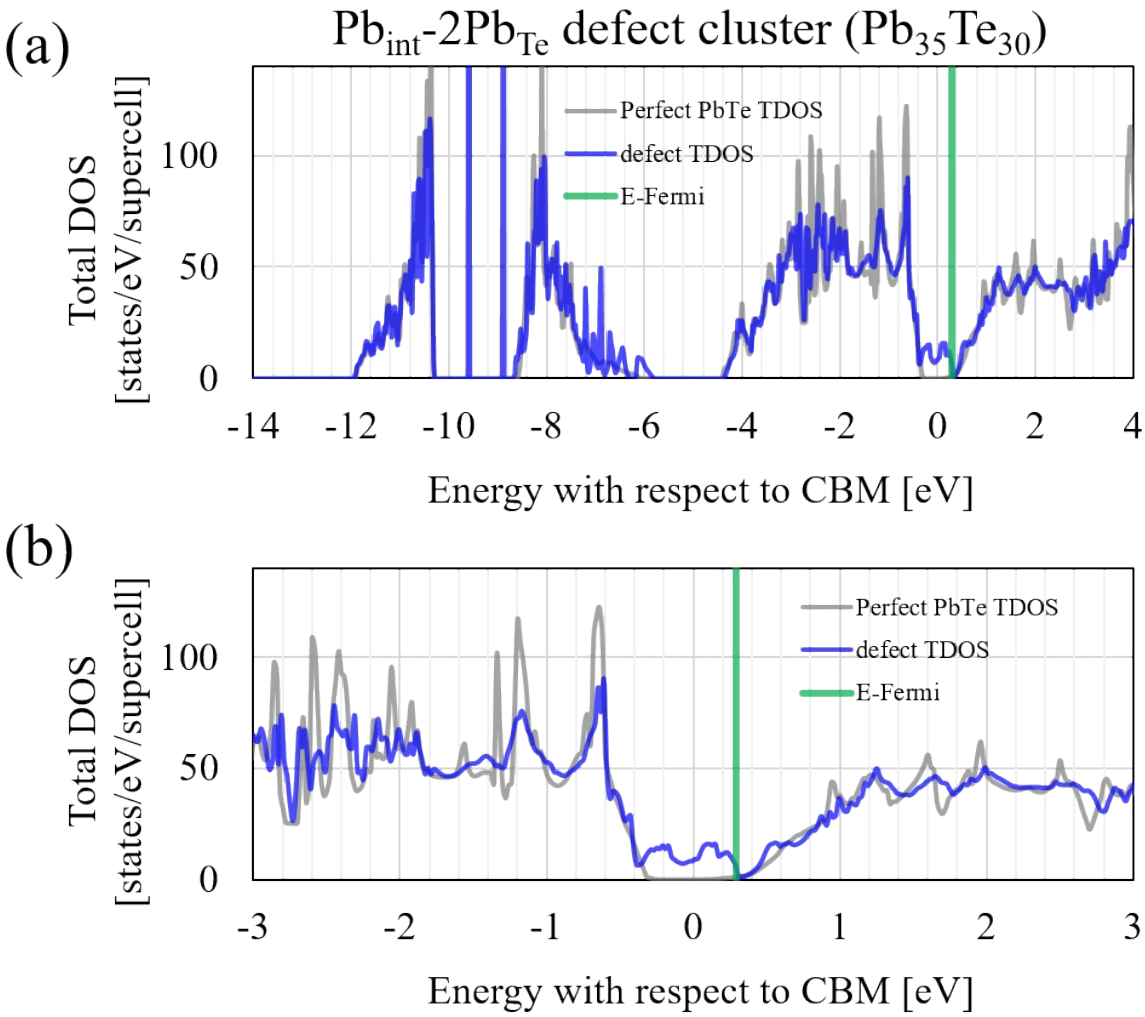

Fig. S9. Total density of states for defect clusters of Pb interstitial and 2 Pb_{Te} antisite defect in PbTe ($Pb_{35}Te_{30}$, blue line) with pristine PbTe (gray line) for comparison with full scale (a) and near the Fermi level (b), where sky blue line is the Fermi level.

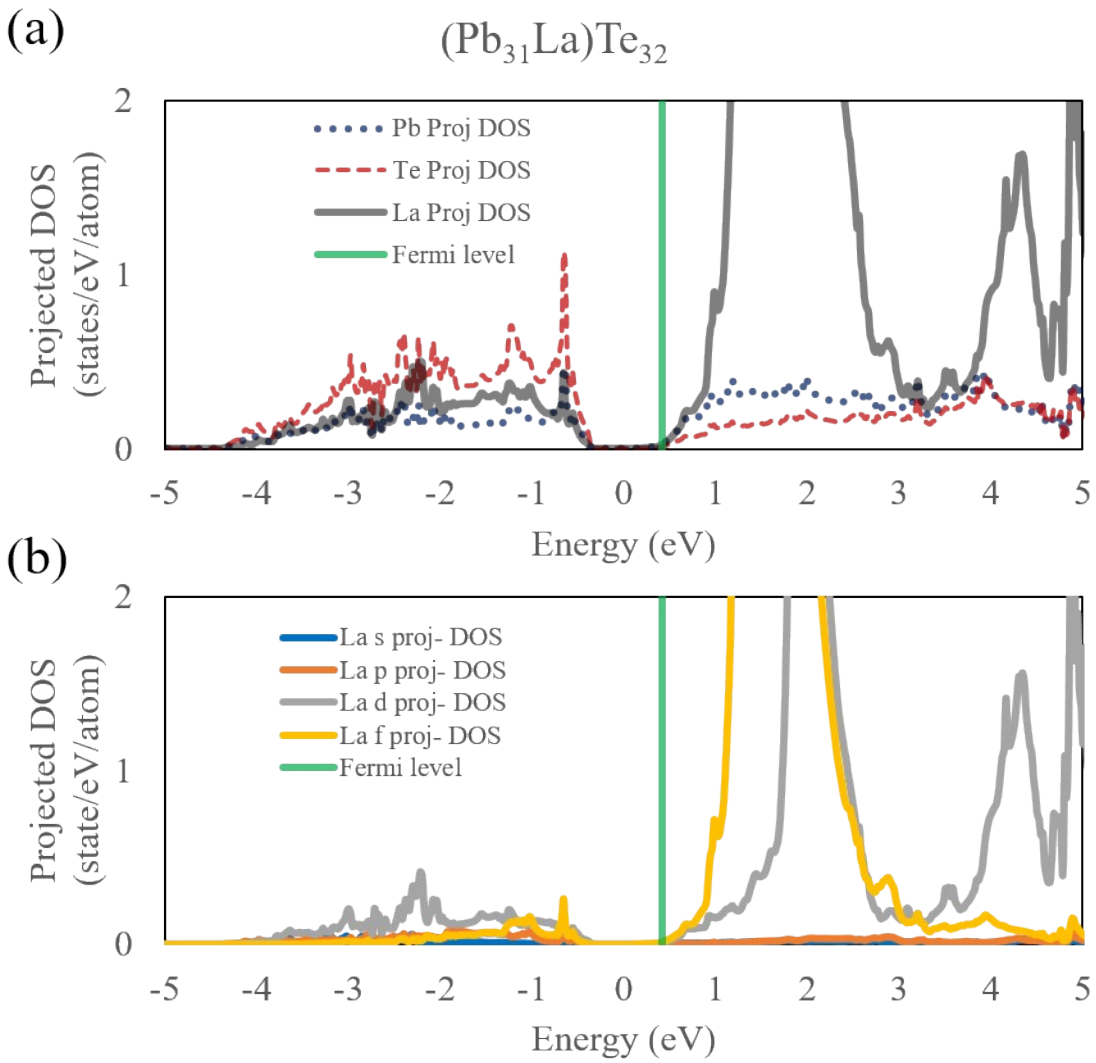

Fig. S10. Pb-, Te-, and La-projected partial density of states in La-doped PbTe ($LaPb_{31}Te_{32}$) (a) and the partial density of states of La-projected ones for each orbitals, where sky blue line is the Fermi level.

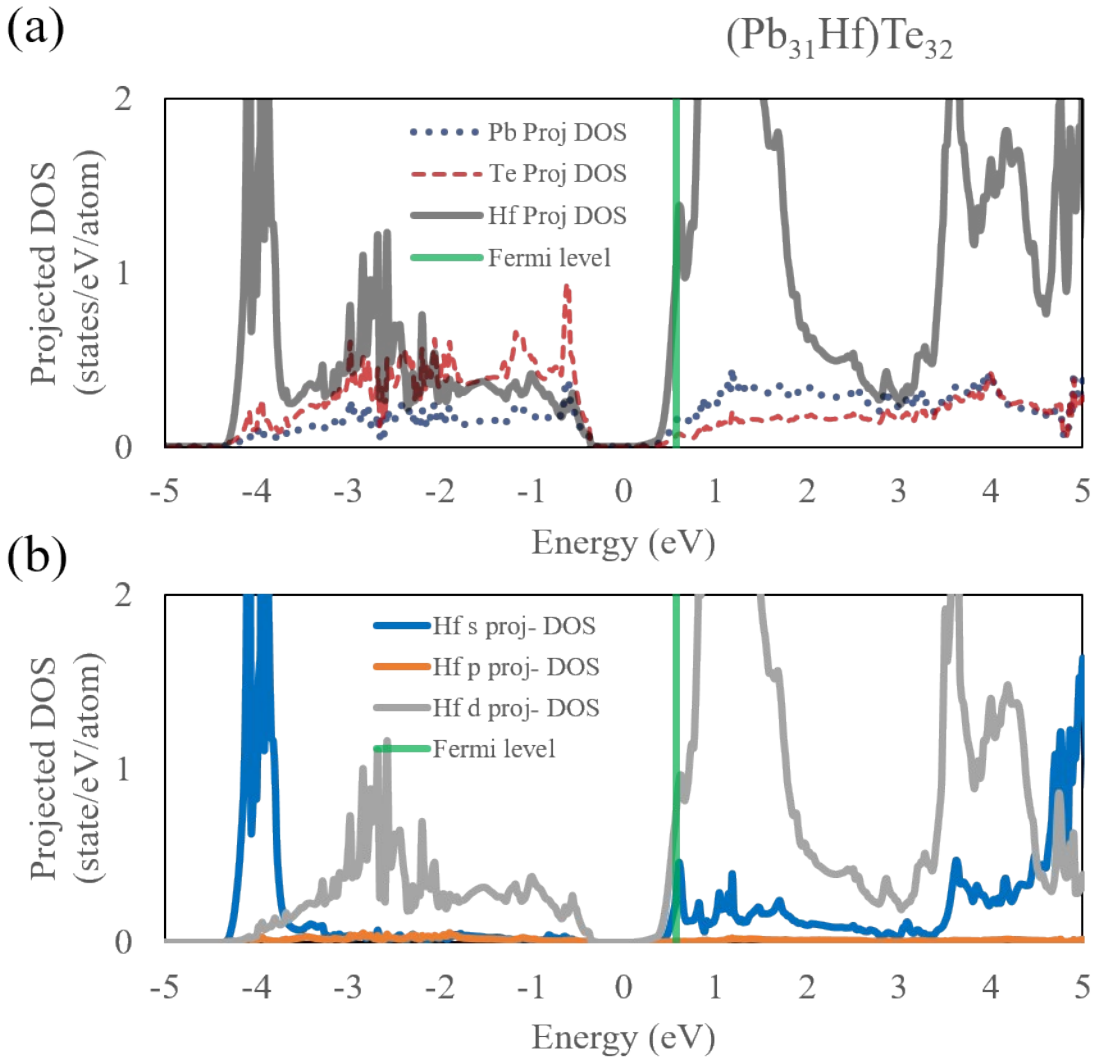

Fig. S11. Pb-, Te-, and Hf-projected partial density of states in Hf-doped PbTe ($HfPb_{31}Te_{32}$) (a) and the partial density of states of Hf-projected ones for each orbitals, where sky blue line is the Fermi level.

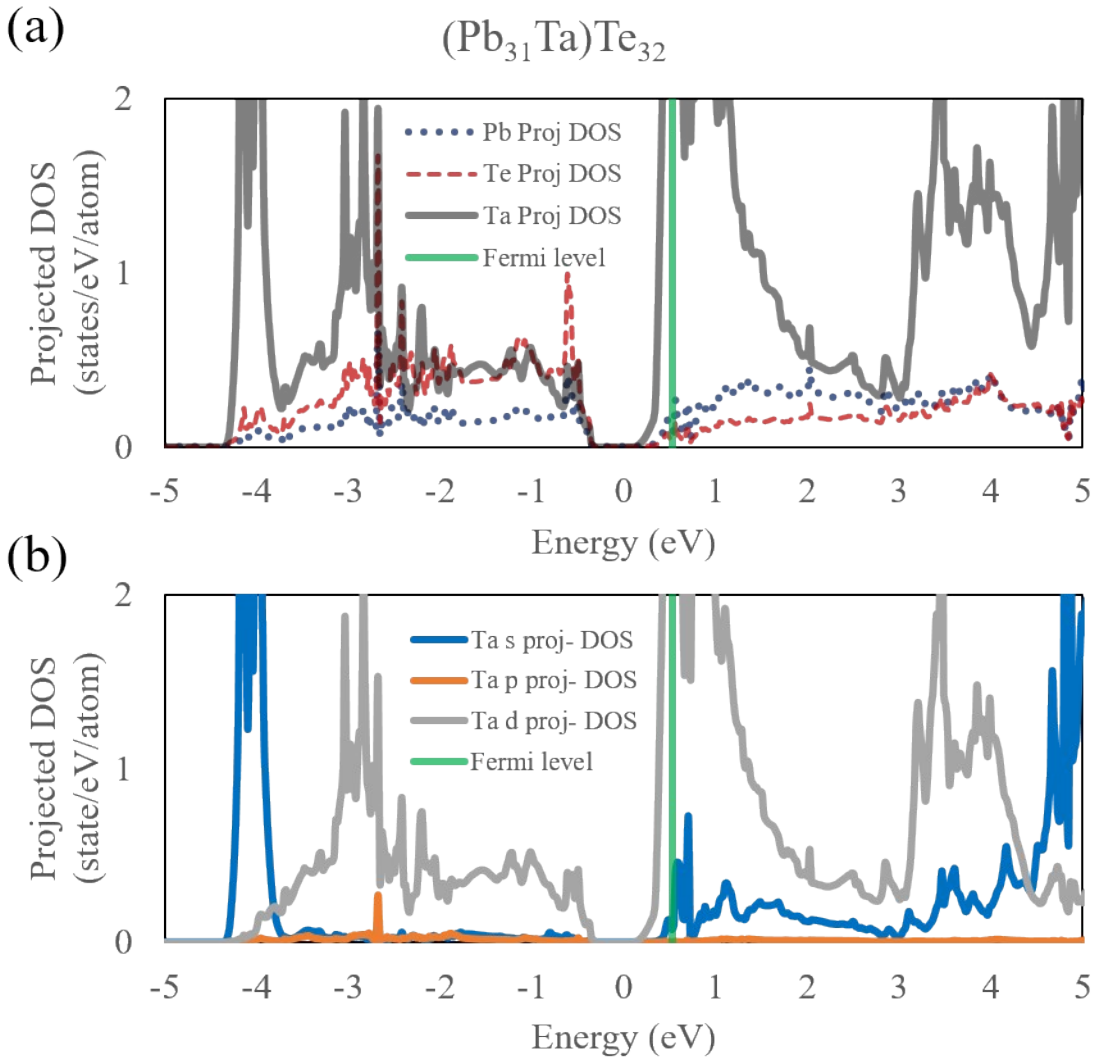

Fig. S12. Pb-, Te-, and Ta-projected partial density of states in Ta-doped PbTe ($TaPb_{31}Te_{32}$) (a) and the partial density of states of Ta-projected ones for each orbitals, where sky blue line is the Fermi level.

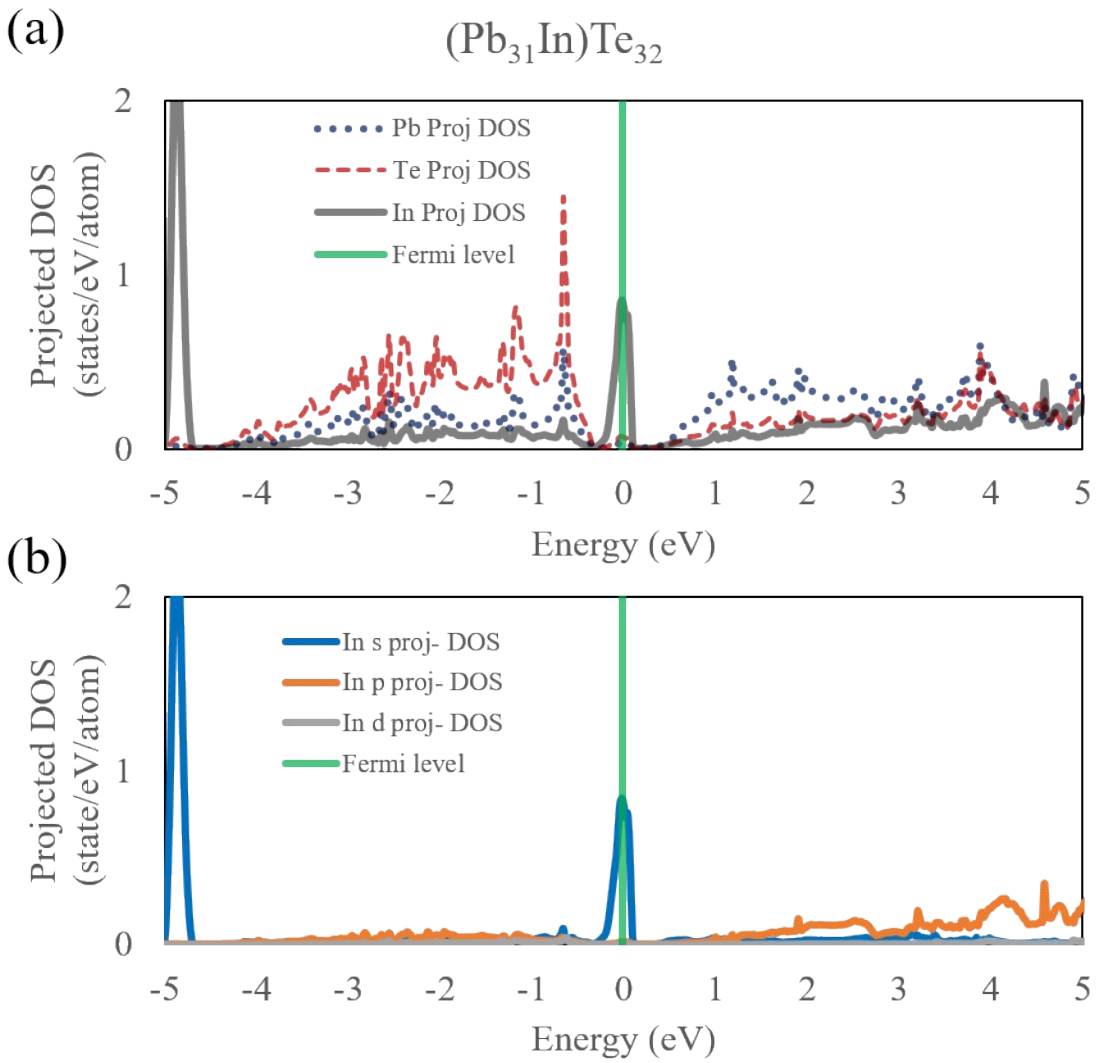

Fig. S13. Pb-, Te-, and In-projected partial density of states in In-doped PbTe ($InPb_{31}Te_{32}$) (a) and the partial density of states of In-projected ones for each orbitals, where sky blue line is the Fermi level.

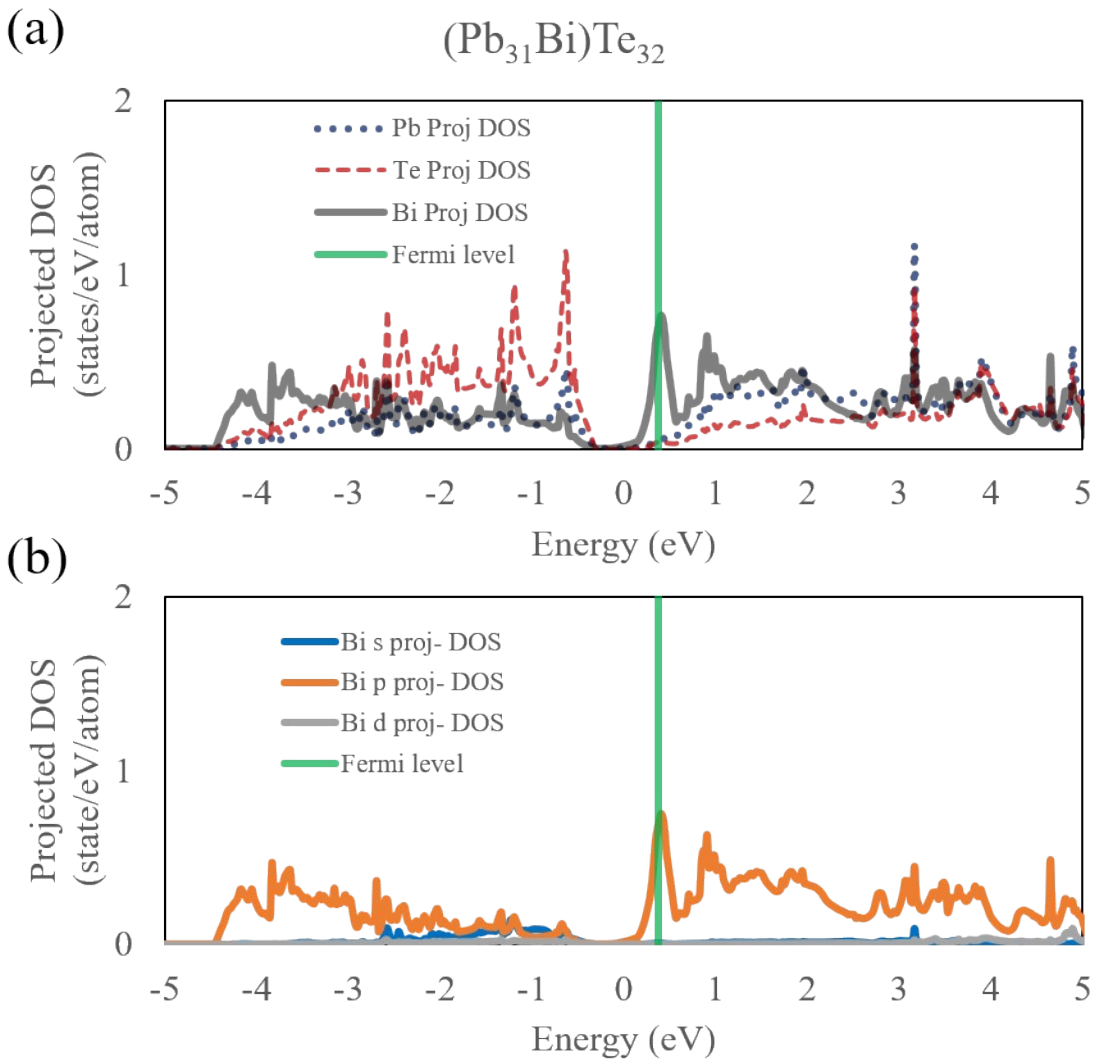

Fig. S14. Pb-, Te-, and Bi-projected partial density of states in Bi-doped PbTe ($BiPb_{31}Te_{32}$) (a) and the partial density of states of Bi-projected ones for each orbitals, where sky blue line is the Fermi level.

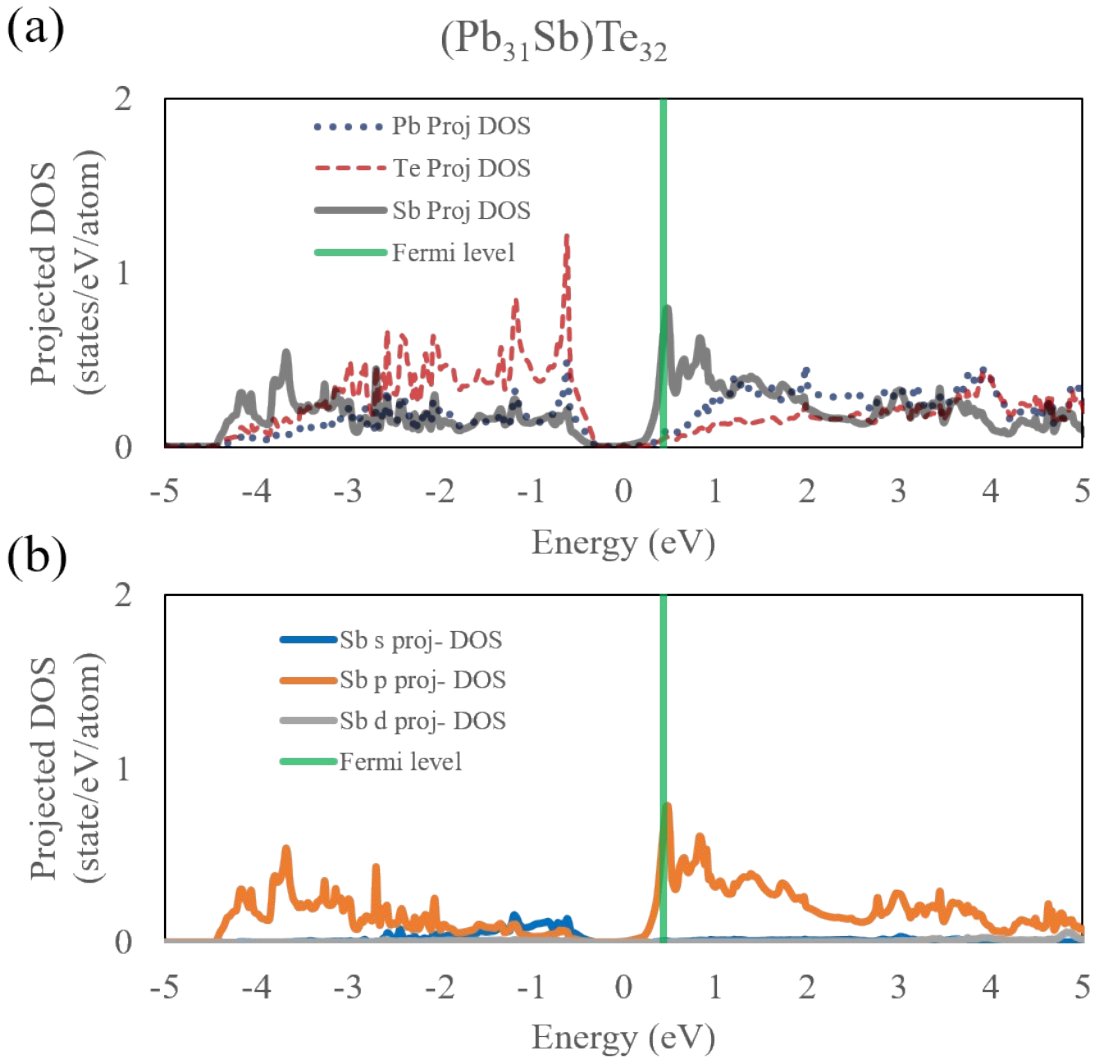

Fig. S15. Pb-, Te-, and Sb-projected partial density of states in Sb-doped PbTe ($SbPb_{31}Te_{32}$) (a) and the partial density of states of Sb-projected ones for each orbitals, where sky blue line is the Fermi level.

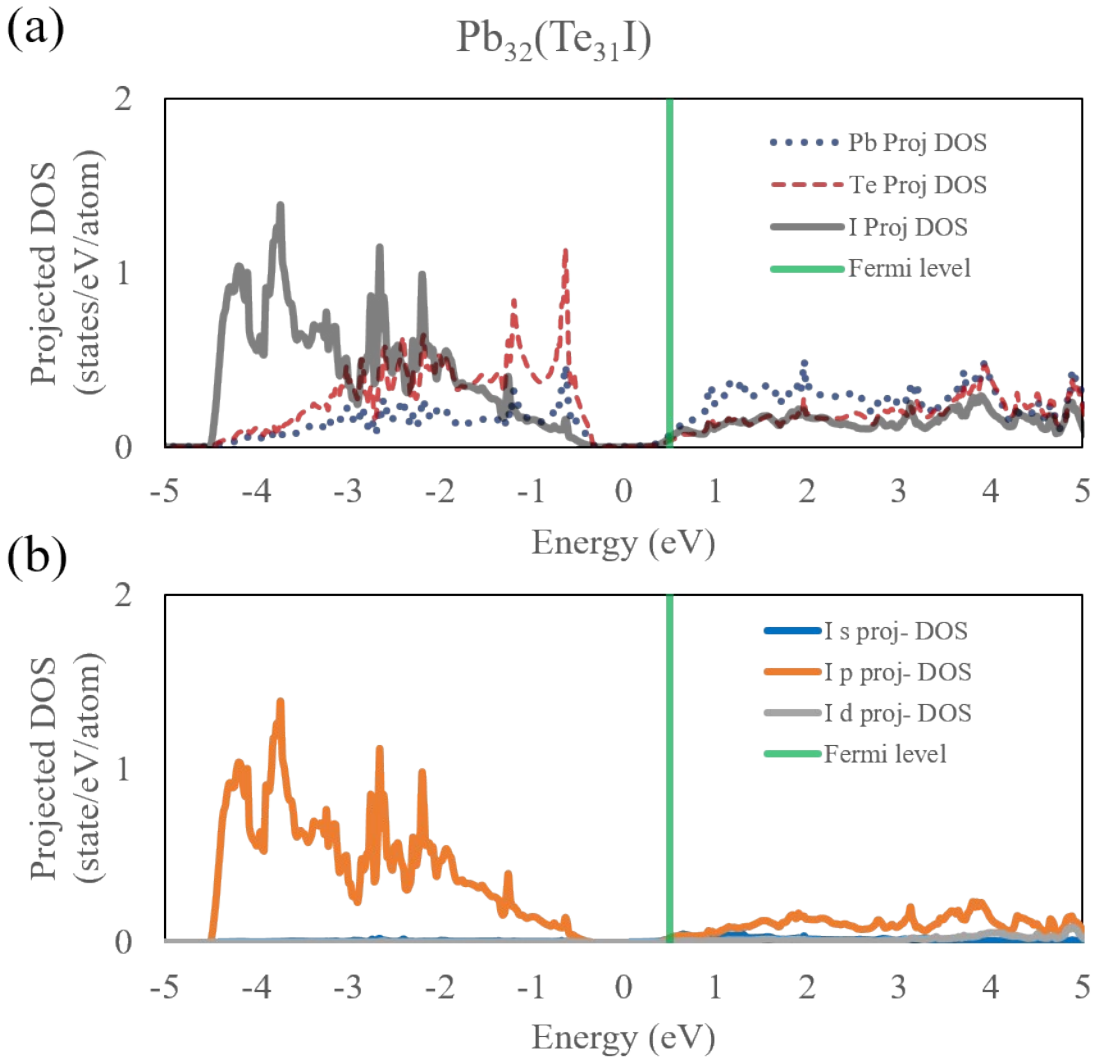

Fig. S16. Pb-, Te-, and I-projected partial density of states in I-doped at Te-site PbTe ($Pb_{32}Te_{31}I$) (a) and the partial density of states of Sb-projected ones for each orbitals, where sky blue line is the Fermi level.

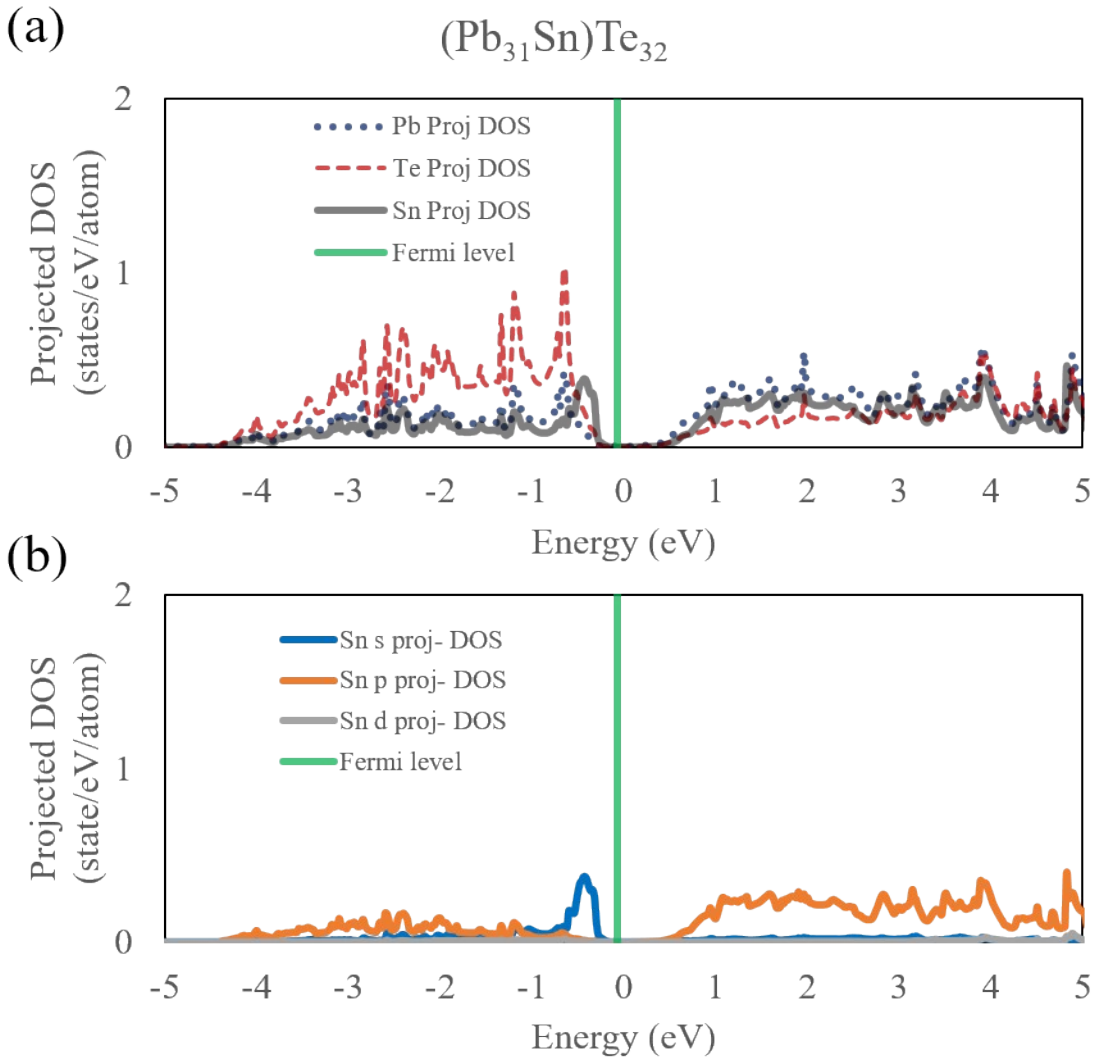

Fig. S17. Pb-, Te-, and Sn-projected partial density of states in Sn-doped PbTe ($SnPb_{31}Te_{32}$) (a) and the partial density of states of Sn-projected ones for each orbitals, where sky blue line is the Fermi level.

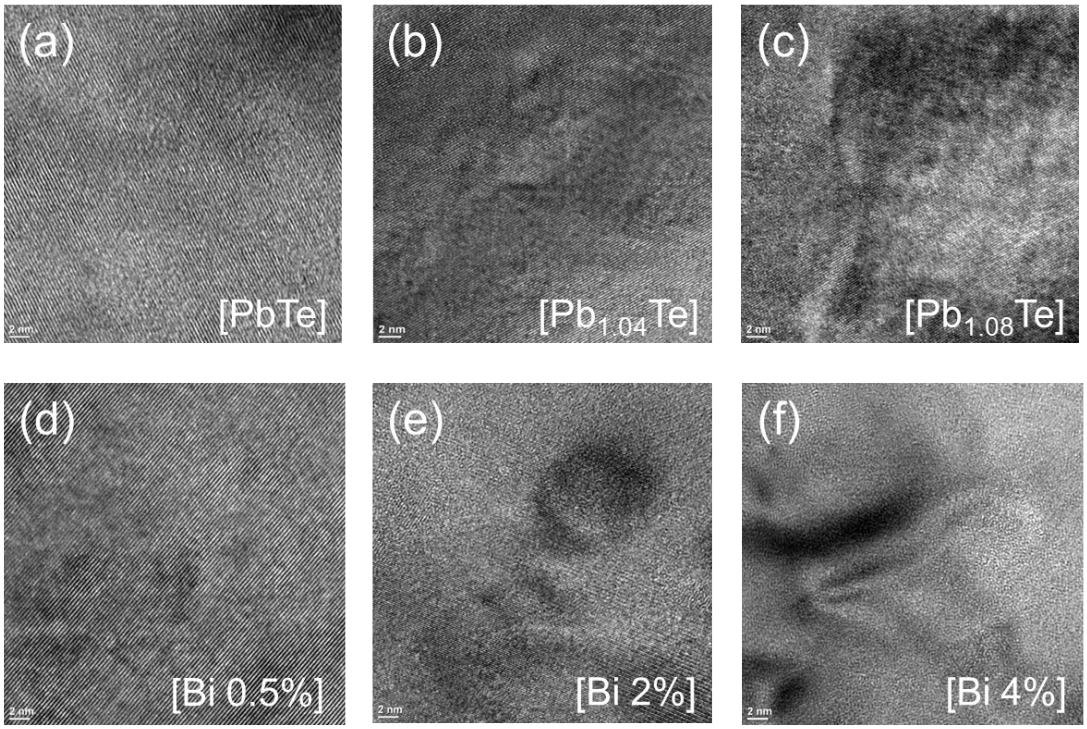

Fig. S18. Transmission electron microscope (TEM) images of pristine PbTe (a), Pb 4 % excess doped PbTe (b), Pb 8 % excess doped PbTe (c), Bi 0.5 % doped $Pb_{0.995}Bi_{0.005}Te$ (d), Bi 2 % doped $Pb_{0.98}Bi_{0.02}Te$ (e), and Bi 4 % doped $Pb_{0.96}Bi_{0.04}Te$ (f).

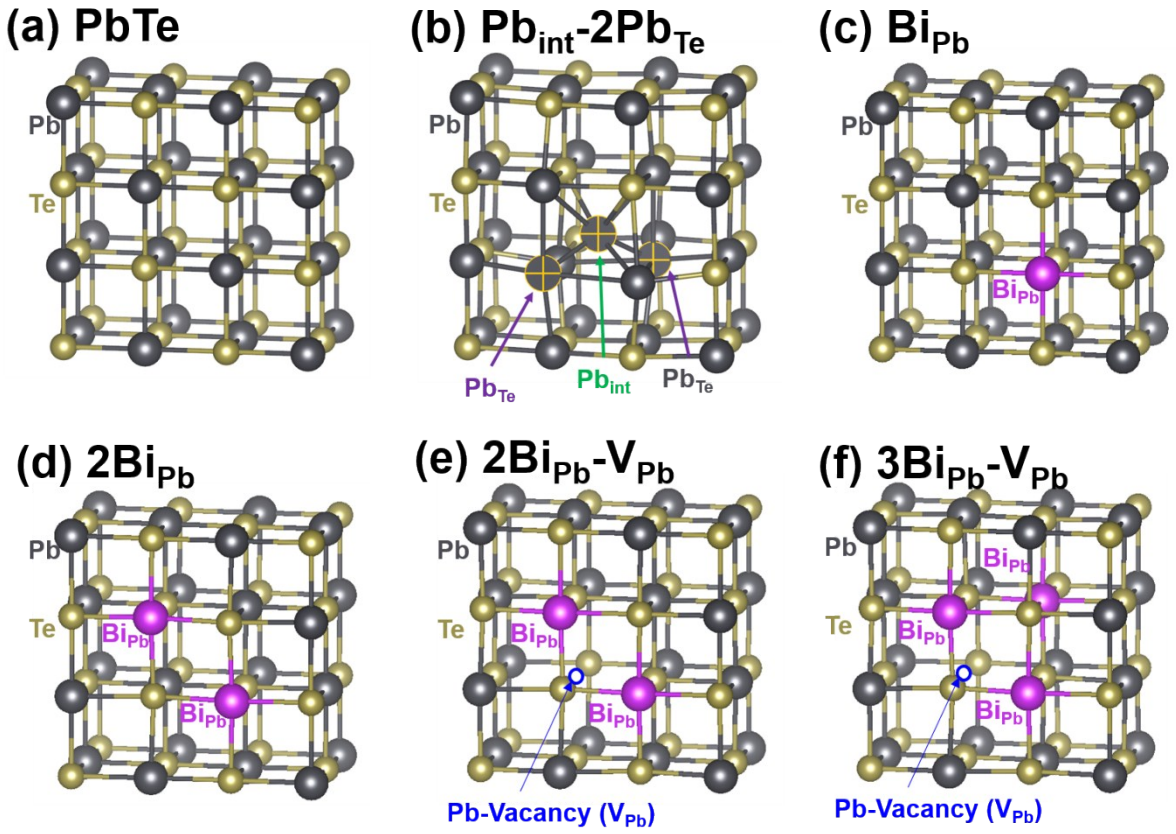

Fig. S19. Representative defect configurations: (a) pristine PbTe, (b) Pb interstitial and 2 Pb atomic substitution in Te site Pb_{int}-$2Pb_{Te}$, (c) Bi doping at Pb site, (d) nearest neighbor Bi pair at Pb site, (e) nearest neighbor Bi pair at Pb-site with Pb vacancy, and (f) 3 Bi atomic substitution at Pb site with one Pb vacancy.

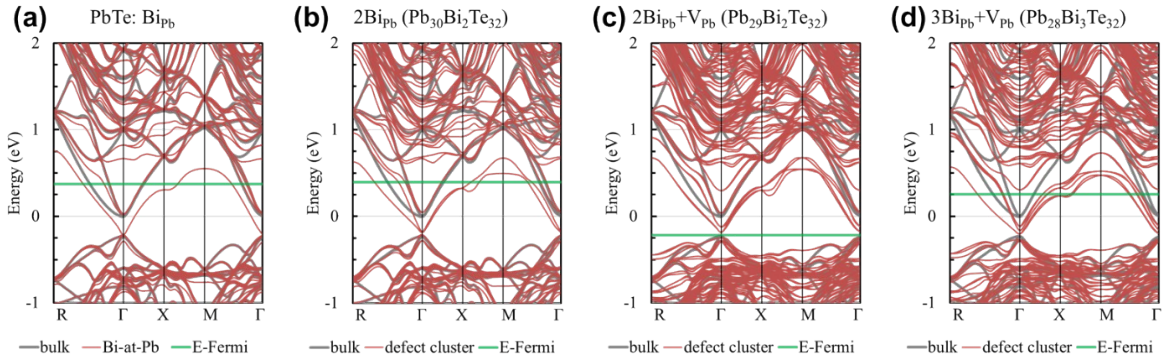

Fig. S20. Band structures of substitutional Bi at Pb (a), nearest neighbor Bi_{Pb} pair (b), $2Bi_{Pb}$-V_{Pb} defect complex (c), and $3Bi_{Pb}$-V_{Pb} defect complex (d).

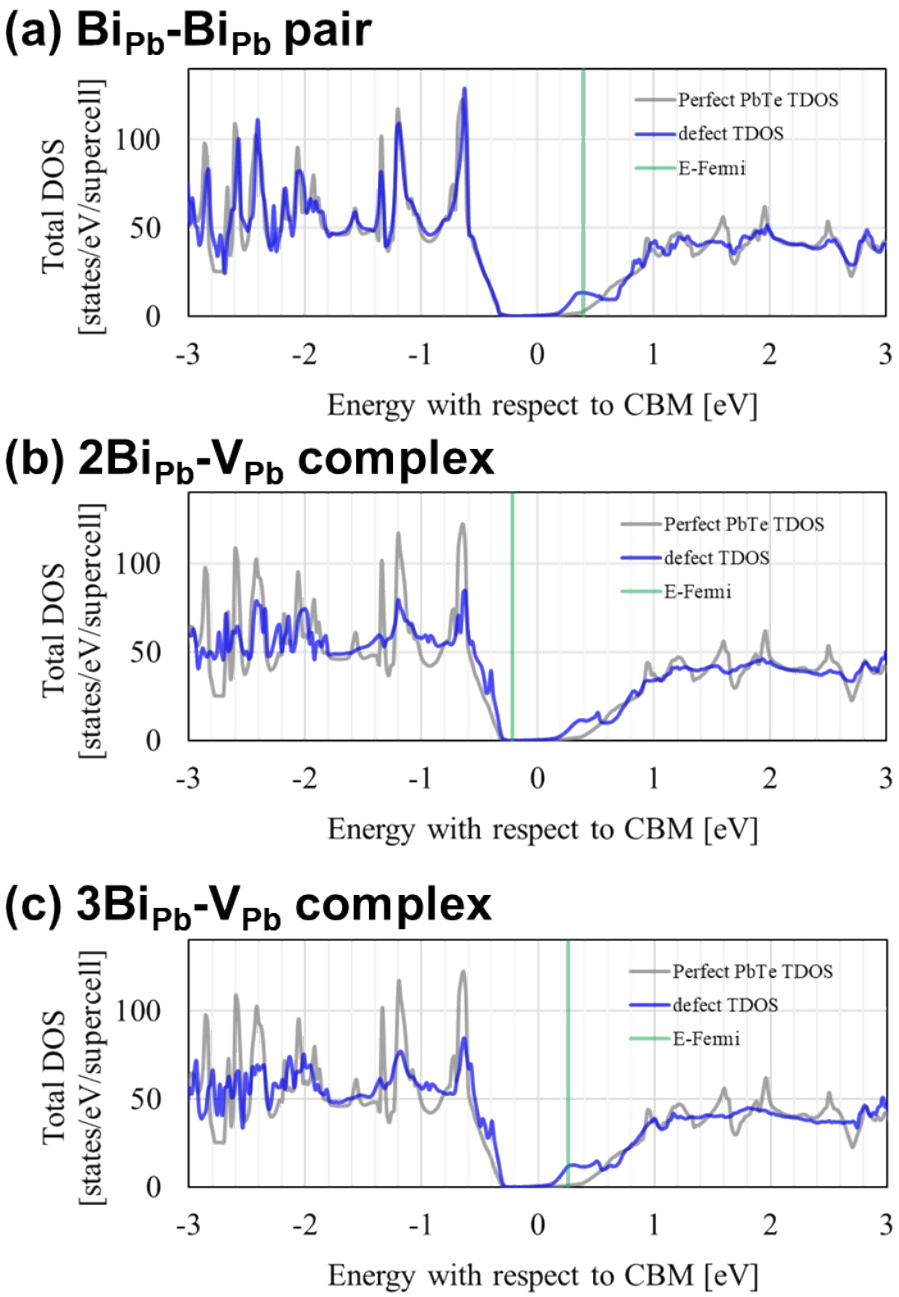

Fig. S21. Density of states of nearest neighbor Bi_{Pb} pair (a), $2Bi_{Pb}$-V_{Pb} defect complex (b), and $3Bi_{Pb}$-V_{Pb} defect complex (c).